Appendix 1

CTP image post-processing

The CTP image reconstruction kernel value was quantum regular 36, with a layer thickness of 3 mm and layer spacing of 2 mm. A commercially available perfusion software for the post-processing workstation (Syngo.via VB10, Siemens Healthineers) was used for CTP reconstruction and preliminary evaluation. Motion correction was applied to all images. A dedicated prototype software (Cardiac Functional Analysis, Siemens Healthineers) was used for MBF evaluation. The MBF lookup table display settings ranged from 0 to 200 mL/100 mL per min for blood flow.

Quantitative evaluation of CTP

The automatic segmentation of the left ventricle was based on a heart model that included the four cardiac chambers. The polar maps were generated based on the 17-segment American Heart Association myocardial model (bulls-eye plots). Manual correction of the contour of the cardiac chambers was performed if the automatic delineation of the chambers was not performed correctly. The MBF lookup table display settings had a range of 0–200 mL/100 mL/min for blood flow.

The value of the quantitative parameters of CTP was measured by a manually drawn volume of interest (VOI) on the MBF polar maps guided by the color-coded scale, with perfusion defects of vessel-based territory. A VOI was drawn on each of the coronary arteries supplying the myocardium; the sizes of the VOIs were at least 0.5 cm^3.

Establishing a mesh model

First, V-Net neural network-based segmentation of the heart chambers (20), including the left myocardium, is conducted in this article. Then, based on neural network image enhancement, multiscale threshold segmentation was used to extract coronary arteries, and operations such as removing veins were performed. After the automatic algorithm, manual editing was also performed to ensure the accuracy of the segmentation.

The reconstruction process from the image segmentation mask to the mesh can be divided into the following steps. First, the input image is preprocessed, and denoising, smoothing, hole filling, and operations are performed to remove abnormal structures caused by pixel discretization. Second, a mesh generation algorithm is used to convert the different scales of the aorta and coronary arteries into mesh grids. This article is based on the Delaunay triangulation method, which is used to generate unstructured meshes (21). Due to the large volume of the aorta, a relatively coarse mesh size can be used, while the coronary artery has a smaller volume and many fine structures, requiring a relatively fine mesh size. Third, the meshes need to be combined and optimized. Combining the aortic and coronary meshes, the generated mesh can be optimized by removing redundant vertices, merging similar vertices, repairing overlapping surfaces, etc., to make the generated mesh more accurate and smoother.

Principle of calculating myocardial blood flow using CTP images

We proposed a method of combining CTA images with CTP images to obtain personalized blood flow information of patients. This method is based on the unit MBF (shown in *Figure S2*) obtained from CTP images. And the hyperemia coefficient is estimated based on the adenosine injection volume, which is used to adjust coronary blood flow for FFR calculations (22).

The CTP images contain a time series of 3 dimensions (3D) CT images. The principle of myocardial perfusion is based on myocardial microcirculation resistance, which can be reflected by the time and concentration of the contrast agent flowing through the myocardium. When the myocardial microcirculation resistance is small, the myocardial blood flow is abundant, the peak time of the contrast agent flow is shorter, and the concentration is higher. When myocardial ischemia occurs, the contrast agent flow time is longer, and the concentration is lower. From this principle, a curve of the contrast intensity of each voxel on the myocardium can be plotted over time, representing the flow of blood containing contrast agents in the myocardial microcirculation. This type of curve is called the tissue attention curve (TAC). Similarly, the curve of the contrast intensity of the aorta over time can also be obtained on CTP images, representing the flow of blood containing contrast agents in the inlet of the coronary artery tree. This curve is called the arterial input function (AIF) curve, as shown in *Figure 3A*.

After obtaining the TAC curve and AIF curve, the corresponding peak-to-peak slope ratio, namely, the MBF, can be calculated using the following formula:

$$MBF = \frac{Max\ Slope\ Tissue\ Attenuation\ Curve(TAC)}{Max\ Artial\ Input\ Function(AIF)} \quad [1]$$

https://dx.doi.org/10.21037/qims-24-2172

The MBF value of each pixel on the myocardium was calculated and converted into a grayscale image to draw the MBF map of the myocardium, as shown in *Figure 3B*.

Each voxel in the figure represents the flow rate at that myocardial location. Based on the flow rate at each voxel, the total flow rate of the entire left ventricular myocardium and the needed blood flow rate for each region of the myocardium can be calculated.

Inclusion and exclusion criteria

Regarding computational fluid dynamics simulations, clear images, accurate segmentation results of blood vessels and chambers, appropriate meshes and accurate boundary conditions are all important factors that directly affect the simulation results. In this article, the clear image mainly includes the edge clarity of the CTA coronary artery and myocardium. On this basis, obtaining accurate segmentation results will more easily result in accurate edges and an improved quality of the mesh model. When the quality of the mesh model is fine, the accuracy of the simulation is mainly determined by the boundary conditions. If the images are too blurry and have severe artifacts, alignment errors and other defects, the recognition of coronary lumens will be affected, and extracting accurate coronary arteries will become difficult. If the patient has undergone stent placement surgery, inaccurate extraction of the lumen within the stent may occur. Patients who have undergone bypass surgery cannot use the method proposed in this article because the blood flow inlet of the coronary artery after bypass surgery increases, which does not meet the boundary condition assumption we made. Other restrictions can be found in Rajiah's research (23).

Correlation between CT-FFR and invasive FFR values and case analysis

The correlation analysis of CT-FFR and invasive FFR values calculated using the above three methods is shown in the following figure (*Figure S1*):

The consistency of the negative CT-FFR values with gold standard (invasive) FFR is higher than that of positive data, and the errors of negative values are smaller. This may be because the coronary lumen of negative data is usually relatively clear and distinguishable, while positive data pose challenges for accurate identification of lumens due to the presence of various soft and hard plaques and stenosis lesions, resulting in significant errors (24).

In terms of the average absolute error, the inlet flow optimization method based on CTP has reduced the average absolute error by 0.033 compared to traditional methods, while the inlet & outlet optimization method based on CTP and blood supply area analysis has only decreased by 0.017 compared to traditional methods. Meanwhile, due to the increased sensitivity of blood supply area analysis to 100% and the decrease in specificity, it is speculated that the method of watershed analysis has led to a more positive result. The reason may be that the outflow ratio of LAD branch by MBF in blood supply area is often more than by Murry's law as shown in section "Inlet flow and outlet flow ratio calculation", which lead more pressure reduce and more positive case in LAD branch, and meanwhile, most invasive FFR measuring position are on the LAD branch.

Figure S2 shows 2 case results to compare the CT-FFR. The top sub figures is one case that the invasive FFR measured on LAD, LCX and right coronary artery (RCA) are all negative values. The CT-FFR calculated by traditional method are all positive as shown in *Figure 2A*, because the myocardium volume is large and the inlet flow is 231.6 mL/min calculated by myocardium. *Figure S2B,S2C* are the new two methods optimized by MBF. The inlet flow calculated by MBF is 139.3 mL/min, smaller than the traditional method, and it make the FFR values negative. The bottom sub figures is another case that the invasive FFR measured on LAD is positive. *Figure S2D-S2F* show the CT-FFR calculated by traditional method, inlet optimization method and inlet & outlet optimization method. The inlet optimization method get negative result as the inlet flow by MBF decrease, however, the inlet & outlet optimization method increases the outlet flow of the LAD branch by the blood supply area analysis and get the right positive result.

The limitations of data collection

The enrollment of 47 CT cases was due to the specific inclusion criteria requiring simultaneous availability of CTA, CTP, and ICA. ICA is an invasive and costly procedure, performed only when necessary, which limits the number of eligible patients. Additionally, in clinical practice, only patients with stable angina who meet specific criteria or those suspected of having myocardial ischemia and hemodynamic abnormalities will undergo the simultaneous completion of CTA, CTP, and ICA. Consequently, the number of eligible patients enrolled in relevant studies is relatively limited.

This study primarily focusing on the initial investigation of innovative technologies. While we recognize that a

https://dx.doi.org/10.21037/qims-24-2172

larger sample size would strengthen our findings, the nature of these procedures and the limited patient availability posed practical challenges. We believe our current sample still provides valuable insights and highlights the need for further research with broader patient recruitment.

The limitations of FFR

ICA derived FFR is the reference standard in this study. As we all known, FFR is the gold standard for determining the need for intervention in stenotic lesions, offering greater sensitivity than ICA for detecting obstructive coronary flow, particularly in stable CAD. However, in unstable CAD, the primary risk is plaque rupture and acute embolism, where FFR may not be low, necessitating additional imaging like OCT or IVUS to assess plaque risk (24). FFR evaluates epicardial stenosis but cannot assess microvascular dysfunction, which may lead to falsely normal FFR values. It also has limitations in diffuse or tandem lesions, potentially underestimating severity. In chronic total occlusion (CTO), FFR may be low despite collateral circulation, and systemic or inflammatory diseases (e.g., vasculitis) can reduce FFR's diagnostic accuracy. FFR requires stable hemodynamics; fluctuations in heart rate or blood pressure, as well as conditions like acute coronary syndrome or arrhythmias, may compromise its reliability.

References

20. Milletari F, Navab N, Ahmadi SA. V-Net: Fully Convolutional Neural Networks for Volumetric Medical Image Segmentation. IEEE 2016.
21. Shewchuk JR. Delaunay Refinement Mesh Generation. Carnegie Mellon University; 1997.
22. Wilson RF, Wyche K, Christensen BV, Zimmer S, Laxson DD. Effects of adenosine on human coronary arterial circulation. Circulation 1990;82:1595-606.
23. Rajiah P, Cummings KW, Williamson E, Young PM. CT fractional flow reserve: a practical guide to application, interpretation, and problem solving. Radiographics 2022;42:340-58.
24. Yan H, Zhao N, Geng YLB. Identification of ischemia-causing lesions using coronary plaque quantification and changes in fractional flow reserve derived from computed tomography across the lesion. Quant Imaging Med Surg 2023;13:3630-43.

Table S1 Statistics results of fractional flow reserve (FFR) calculating by the coronary inlet and outlet flow optimization through MBF by patients

FFR calculation method	Accuracy	Sensitivity	Specificity
Traditional method	87.2%	92.0%	81.8%
Inlet flow optimization method	89.4%	88.0%	90.9%
Inlet & outlet flow optimization method	93.6%	100%	86.4%

FFR, fractional flow reserve; MBF, myocardial blood flow.

https://dx.doi.org/10.21037/qims-24-2172

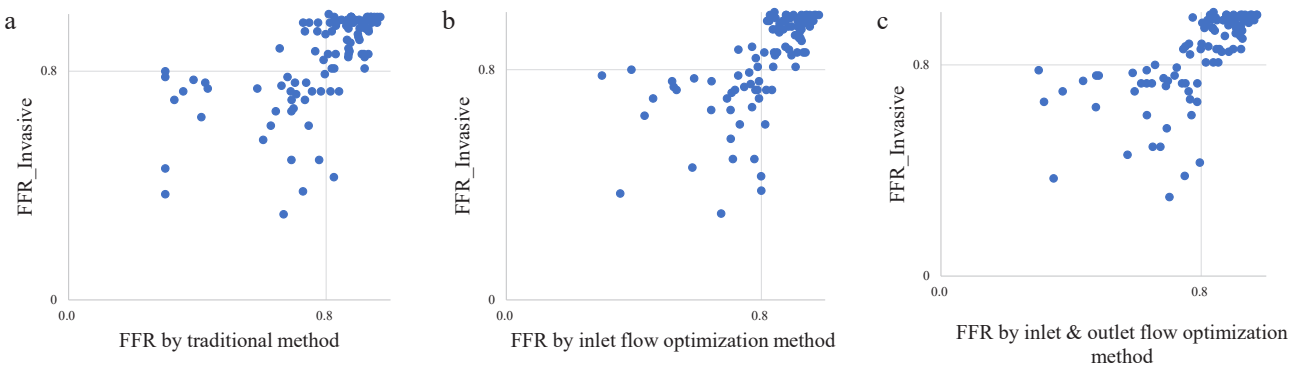

Figure S1 Correlation of computed tomography angiography-derived fractional flow reserve (CT-FFR) to fractional flow reserve (FFR)-invasive.

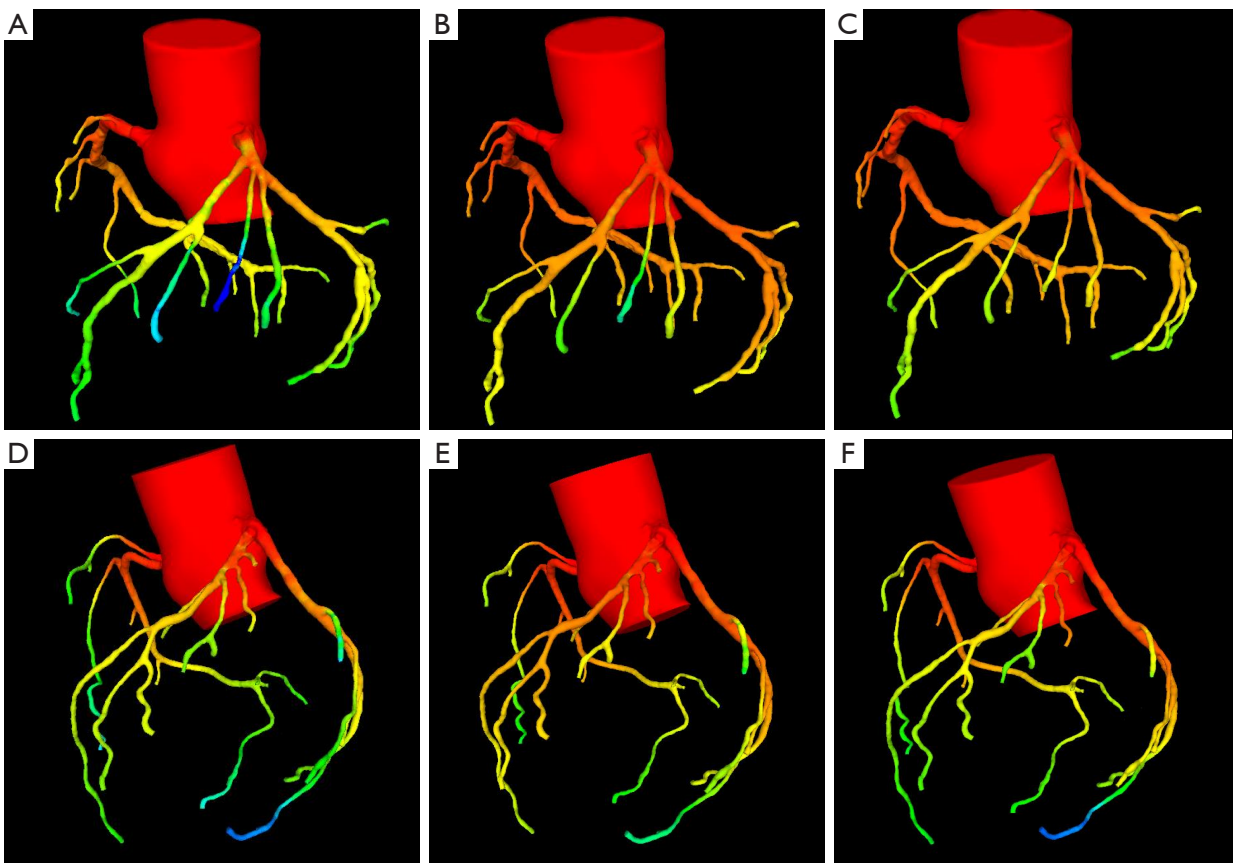

Figure S2 Fractional flow reserve (FFR) results of 2 cases by 3 methods. (A-C) The first case and (D-F) the second case. (A,D) The FFR results by traditional method, (B,E) inlet optimization method and (C,F) inlet & outlet optimization method.

https://dx.doi.org/10.21037/qims-24-2172

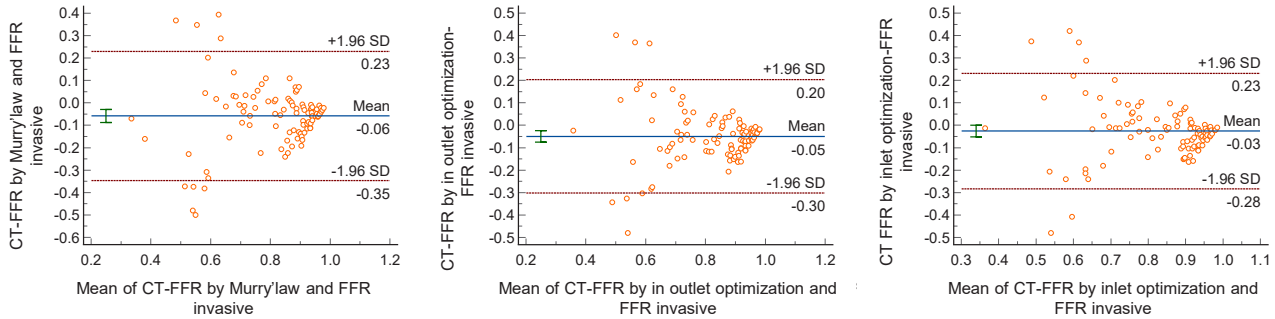

Figure S3 B-A plot of the three CT-FFR calculation method compare to the FFR-invasive. CT-FFR: computed tomography angiography-derived fractional flow reserve.

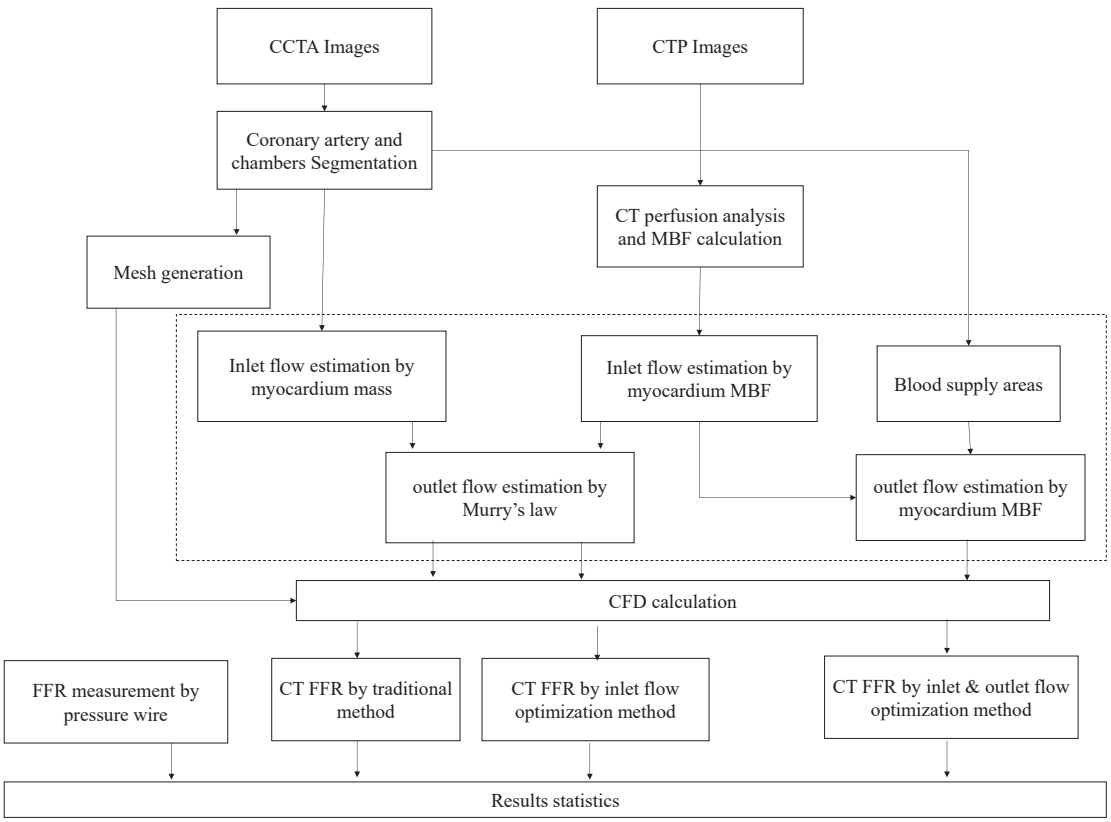

Figure S4 Flow char of CT-FFR and the optimization methods by MBF. CT-FFR: computed tomography angiography-derived fractional flow; MBF: myocardial blood flow reserve.

https://dx.doi.org/10.21037/qims-24-2172